Enhanced conductivity in pulsed laser deposited Ce0.9Gd0.1O2/SrTiO3 heterostructures

Kant, K. Mohan; Esposito, Vincenzo; Pryds, Nini

Published in:
Applied Physics Letters

Link to article, DOI:
10.1063/1.3497294

Publication date:
2010

Document Version
Publisher's PDF, also known as Version of record

Enhanced conductivity in pulsed laser deposited $Ce_{0.9}Gd_{0.1}O_{2-\delta}/SrTiO_3$ heterostructures

K. Mohan Kant, V. Esposito, and N. Pryds[a)]
Fuel Cells and Solid State Chemistry Division, Risø Denmark Technical University, Roskilde-4000, Denmark

(Received 5 July 2010; accepted 15 September 2010; published online 5 October 2010)

Significant enhancement in the electrical conductivity of $Ce_{0.9}Gd_{0.1}O_{2-\delta}$ (CGO) thin films (250 and 500 nm) deposited on MgO(001) substrate is observed by introducing ~50 nm thin $SrTiO_3$ buffer layer film. Introduction of the buffer layer is found to form epitaxial films, leading to minimal grain boundary network that results in a free conduction path with near-zero blocking effects perpendicular to current flow. The in-plane conductivity measurements confirm increase in conductivity with increase in compressive strain on CGO films. © *2010 American Institute of Physics*. [doi:10.1063/1.3497294]

Gadolinium doped ceria is a well-known oxygen ionic conductor for applications such as solid oxide fuel cells (SOFCs), gas sensors, and gas separation membranes.[1–3] $Ce_{0.9}Gd_{0.1}O_{2-\delta}$ (CGO) exhibit larger ionic conductivity than yttrium stabilized zirconia, the conventional fuel cell electrolyte.[4,5] There is a huge interest to obtain ionic thin films with less Ohmic resistance, scaling linearly with thickness, thus operating at lower temperature.[6] CGO deposited on substrates like MgO(001), $LaAlO_3$(001), $NdGaO_3$(001), Si(001), and $SrTiO_3$(001) results in polycrystalline or epitaxial thin film.[7–13] From the view point of electrical transport, MgO(001) can be regards as insulator (resistance R $=10^9$ Ω at 800 °C) even at high temperatures thus making it a near-ideal substrate to evaluate electrical properties.[14] However, CGO thin films on MgO(001) are polycrystalline due to large lattice misfit between substrate and film ($|a_{CGO}-a_{MgO}|/a_{CGO}\times 100=9.1\%$) resulting in blocking effects due to the large density of grain boundary network.[15,16] The lattice mismatch between $SrTiO_3$ (STO) and CGO reduces to ~1.9% ($|a_{CGO}-a_{STO}|/a_{STO}\times 100=1.9\%$) by 45° in-plane rotation of CGO with respect to STO resulting in epitaxial films.[10] The major difficulty in thin film conductivity measurements is to separate the contribution of the substrate from the total measured resistance and evaluate the film conductivity. However, polycrystalline STO shows electronic conductivity only above 300 °C in reducing conditions, and Sanna *et al.*[10] have shown that for 20% molar samaria doped ceria (SDC) deposited on STO buffer layer-MgO (SDC/STO/MgO) the electronic contribution of STO is negligible for high pO_2 values. In this work, conductivity of CGO films with different thickness (250 and 500 nm) were deposited on MgO(001) and MgO(001)/$STO_{50\ nm}$ measured in air, where CGO is pure ionic conductor and the substrate contribution [MgO(001) and MgO(001)/$STO_{50\ nm}$] is negligible. STO buffer layer (lattice parameter a=b=c=3.907 Å) was deposited as 50 nm thick film on MgO in order to ensure epitaxial growth of CGO (a=b=c=5.418 Å) on MgO(001) (a=b=c=4.219 Å) substrate. Similar approach was successful in obtaining epitaxial superconducting $YaBa_2Cu_3O_{7-\delta}$ (YBCO) thin films on MgO (001) and chemical and thermally stable $Ce_{0.8}Sm_{0.2}O_{2-\delta}$ on MgO.[10,17,18]

CGO target was prepared from commercial powder (Rhodia, Purity 99.99%) by 120 MPa uniaxial pressure followed by sintering at 1500 °C for 24 h. Pulsed laser deposition using KrF laser (248 nm) was used to deposit STO (50 nm) and CGO (250 and 500 nm) thin films on MgO(001) substrate. STO films were deposited at oxygen partial pressure P_{O_2} of 0.1 mbar, maintaining substrate temperature at 760 °C, and frequency of 2 Hz. After the deposition the STO film was cooled to room temperature at 10 °C per min rate in 1 mbar P_{O_2}. Similarly, CGO films were deposited at P_{O_2} of 10^{-2} mbar, substrate temperature of 750 °C, and frequency of 10 Hz with a cooling rate of 10 °C per min. Growth rate was 0.8 nm/min (2 Hz) and 4 nm/min (10 Hz) for the STO and CGO thin films respectively. The electrical properties were studied by both AC impedance and two-probe dc techniques in the temperature range 450–900 °C in air using gold (Au) current collectors onto $La_{0.6}Sr_{0.4}MnO_{3-\delta}$ (LSM) electrodes deposited onto the GCO film surface. LSM electrodes have high electronic conductivity and thermal expansion and ensure perfect adherence and full coverage of CGO at all temperatures. Au current collectors were deposited on LSM and annealed at 1000 °C for 12 h prior to the measurements for good contact formation. The impedance spectra were correlated with dc measurements to monitor electrode contribution.

Figures 1(a) and 1(b) show x-ray diffraction (XRD) patterns from representative MgO(001)/$STO_{50\ nm}$ and MgO(001)/$STO_{50\ nm}$/$CGO_{250/500\ nm}$ films. These reveal the cubic fluorite structure of CGO films deposited on MgO(001)/$STO_{50\ nm}$ with no evidence of secondary phases. Only (*h*00) diffraction peak was detected indicating that the epitaxially grown $STO_{50\ nm}$ film with [100] direction perpendicular to substrate surface [Fig. 1(b)].

The lattice constant (α) of STO film is 3.924 Å, slightly larger than that in bulk STO (3.907 ± 0.001 Å), showing that the $STO_{50\ nm}$ film is in-plane compressed. The relative strain (s) is estimated from the relation, $s=(\alpha-\alpha_{bulk})/\alpha_{bulk}$, where α_{bulk} is the lattice constant of bulk. $STO_{50\ nm}$ film exhibited 0.45% strain leading to misfit of 2.3% between $STO_{50\ nm}$ buffer layer and CGO film. Similarly $CGO_{250\ nm}$ and

a)Author to whom correspondence should be addressed. Electronic mail: nipr@risoe.dtu.dk.

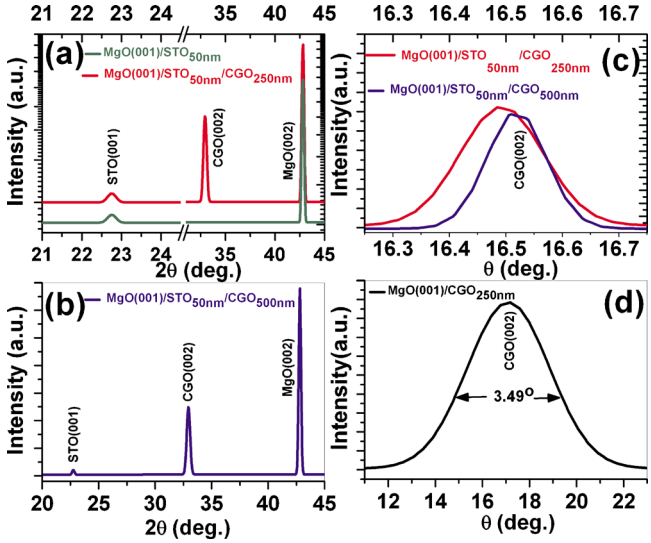

FIG. 1. (Color online) The θ-2θ scans of (a) MgO(001)/$STO_{50\ nm}$, MgO(001)/$STO_{50\ nm}$/$CGO_{250\ nm}$ and (b) MgO(001)/$STO_{50\ nm}$/$CGO_{500\ nm}$. Rocking curves of (002) reflection of CGO in (c) MgO(001)/$STO_{50\ nm}$/$CGO_{250\ nm}$ and MgO(001)/$STO_{50\ nm}$/$CGO_{500\ nm}$, and (d) MgO(001)/$CGO_{250\ nm}$.

$CGO_{500\ nm}$ films deposited on MgO/$STO_{50\ nm}$ resulted in 0.12% and 0.09% strain in CGO lattice. These small values of strain indicate higher structural coherence in CGO films deposited on $STO_{50\ nm}$ buffer layer. However, the FWHM value obtained from rocking curves of (002) for CGO films deposited directly on MgO substrate (3.49°) is one order larger than for the films deposited on MgO using a STO buffer layer (0.21°) [Figs. 1(c) and 1(d)]. This observation clearly demonstrates that $STO_{50\ nm}$ buffer layer improves the lattice match between MgO and CGO by inducing strain on CGO (0.12% and 0.09%) film. No strain is observed in polycrystalline CGO films deposited on MgO(001) under the same conditions.

The Φ scan on (301) peak of STO in MgO(001)/$STO_{50\ nm}$ films show four distinct peaks with same intensity and nearly 90° spacing between peaks (Fig. 2). Similar trend was observed for CGO(311) reflection, with a displacement of 45° with respect to MgO(311). Epitaxial

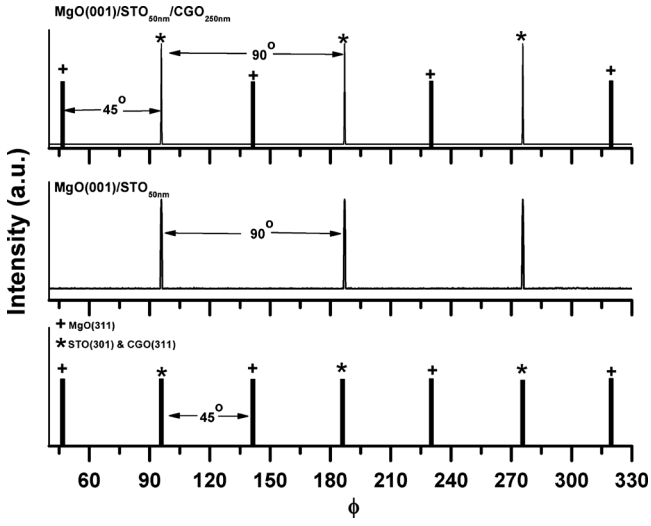

FIG. 2. The Φ scan XRD patterns of MgO(001)/$STO_{50\ nm}$/$CGO_{250\ nm}$ and MgO(001)/$STO_{50\ nm}$ heterostructures.

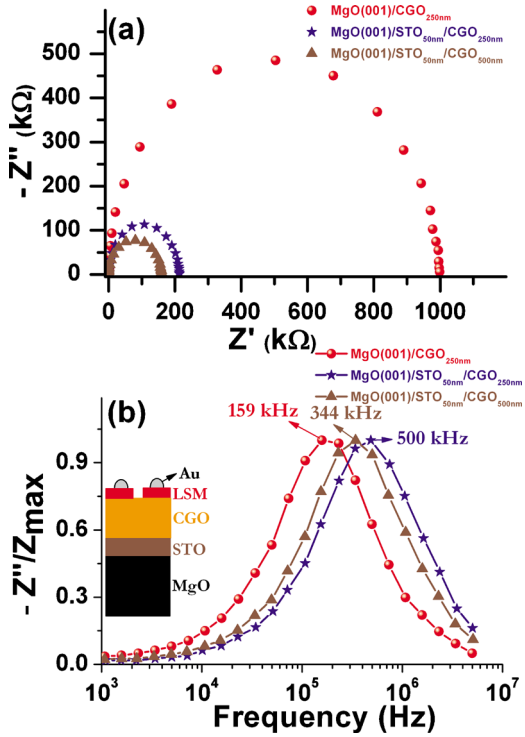

FIG. 3. (Color online) (a) Nyquist plot and (b) frequency dependence of imaginary part impedance for measured in air at 400 °C for MgO(001)/$CGO_{250\ nm}$, MgO(001)/$STO_{50\ nm}$/$CGO_{250\ nm}$, and MgO(001)/$STO_{50\ nm}$/$CGO_{500\ nm}$. Inset is electrodes arrangement used for *in-plane* conductivity measurements.

growth of CGO(001) on MgO(001) with $STO_{50\ nm}$ buffer layer has been achieved through rotation of CGO lattice by 45° with respect to STO lattice. This clearly indicates that epitaxial CGO films were realized on $STO_{50\ nm}$ basal plane (5.548 Å) due to low misfit compared to MgO(001). The XRD patterns of MgO/$STO_{50\ nm}$/$CGO_{250/500\ nm}$ heterostructures taken after electrical transport measurements at high temperature showed that the films retained their crystalline quality and, most important, the CGO is perfectly coherent with the STO, in agreement with XRD results, meaning that the $CGO_{250\ nm}$ layer grows rotated by 45° around the *c* axis and strains to match the STO basal plane. Increasing CGO thickness to 500 nm, it resulted in lowering of strain to 0.09%.

Figure 3(a) shows impedance spectra measured in air at 400 °C for MgO(001)/$CGO_{250\ nm}$, MgO(001)/$STO_{50\ nm}$/$CGO_{250\ nm}$, and MgO(001)/$STO_{50\ nm}$/$CGO_{500\ nm}$ films. The spectra consist of a single nondepressed semicircles and no electrode feature is apparent in the spectra because their low impedance contribution. A single RC element (i.e., a resistor in parallel with a capacitor) is used as equivalent circuit to obtain the impedance-frequency relation at various temperatures. A single impedance arc of the polycrystalline CGO thin films is ascribed to total contribution of the grains and grain boundaries to the ionic conductivity. The total resistance of the sample is measured as the diameter of the semicircle. Frequency distribution shows the RC relaxation times for the samples at 400 °C [Fig. 3(b)]. CGO films deposited on MgO(001)/$STO_{50\ nm}$ at 400 °C in air relax faster (10^{-7} s) compared to those deposited on MgO(001) substrate (10^{-6} s). The resistance measured by two probe dc method

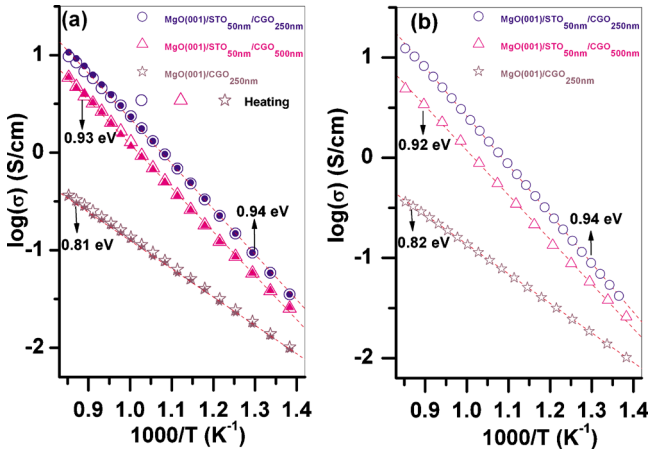

FIG. 4. (Color online) Conductivity vs temperature plots for $MgO(001)/CGO_{250\ nm}$, $MgO(001)/STO_{50\ nm}/CGO_{250\ nm}$, and $MgO(001)/STO_{50\ nm}/CGO_{500\ nm}$ obtained from (a) Nyquist plots and (b) two probe dc measurement. Open and closed symbols correspond to the data obtained during heating and cooling cycles. Dotted lines correspond to linear fit.

is nearly equal to the value of resistance obtained from the impedance spectrum due to the low contribution of the electrodes polarization. No thermal hysteresis was observed in $MgO(001)/CGO_{250\ nm}$, $MgO(001)/STO_{50\ nm}/CGO_{250\ nm}$, and $MgO(001)/STO_{50\ nm}/CGO_{500\ nm}$ heterostructures. The capacitance value obtained for heterostructures are $\sim 10^{-11}$ F and is of the order of the stray capacitance i.e., C value might not be characteristic of CGO polycrystalline bulk material but it is typical of doped-ceria in thin film shape.[10] Figure 4 shows Arrhenius plots of $MgO(001)/CGO_{250\ nm}$ and $MgO(001)/STO_{50\ nm}/CGO_{250/500\ nm}$ films measured in the temperature range of 450 to 900 °C in air. The activation energy (E_a) of $MgO(001)/CGO_{250\ nm}$ was calculated to be ~0.81 and 0.82 eV from Nyquist plots [Fig. 4(a)] and dc two probe [Fig. 4(b)] measurements. The activation values are in the range of 0.8–0.9 eV as obtained for polycrystalline CGO films.[14,19,20] The slight increase in the dc measurements in the entire temperature range were attributed to the contribution of electrodes adherent to the CGO film surface. At 450 °C, CGO films deposited on $MgO(001)/STO_{50\ nm}$ exhibit fivefold larger conductivity than in the films deposited on MgO(001) substrate. At 900 °C, total conductivity is found to be 3.7×10^{-1} S/cm, 5.1 S/cm, and 12.1 S/cm for $MgO(001)/CGO_{250\ nm}$, $MgO(001)/STO_{50\ nm}/CGO_{500\ nm}$, and $MgO(001)/STO_{50\ nm}/CGO_{250\ nm}$ samples, respectively. The conductivity curves shift upwards in films with $STO_{50\ nm}$ buffer layer. The calculated activation energies for $MgO(001)/STO_{50\ nm}/CGO_{250/500\ nm}$ films were 0.93 and 0.94 eV. These activation energies correspond to the values reported for bulk doped ceria.[21]

For coherent epitaxial growth, the lattice mismatch between thin film and substrate is accommodated entirely by strain within the film. As the film grows thicker the total strain energy in the film increases rapidly. The relaxation of this strain field determines the final film crystallinity. Mostly, the strain field caused by the lattice mismatch will be relaxed by generating dislocations and local lattice distortions, distribution of which strongly influence the film crystallinity. Large regions of lattice distortions may result in a columnar or polycrystalline growth, degrading the film quality and thus reducing the conductivity.[9,22,23] In our $MgO(001)/STO_{50\ nm}/CGO_{250/500\ nm}$ heterostructures, the presence of uniformly strained regions lead to epitaxial nearly single crystal films. The increase in conductivity is attributed to negligible number of grain boundaries perpendicular to current flow. Conductivity enhancements open up exciting opportunities for oxide ionic conductors in technologies such as SOFCs.

[1] U. P. Muecke, D. Ceckel, A. Bernard, A. Bieberle-Hutter, S. Graf, A. Infortuna, P. Muller, J. L. M. Rupp, J. Schneider, and L. J. Gauckler, Adv. Funct. Mater. **18**, 3158 (2008).
[2] X. Chen, N. J. Wu, L. Smith, and A. Ignatiev, Appl. Phys. Lett. **84**, 2700 (2004).
[3] J. Will, A. Mitterdorfer, C. Kleinlogel, D. Perednis, and L. J. Gauckler, Solid State Ionics **131**, 79 (2000).
[4] B. C. H. Steele, Solid State Ionics **129**, 95 (2000).
[5] J. A. Kilner, Solid State Ionics **129**, 13 (2000).
[6] J. A. Kilner, Nature Mater. **7**, 838 (2008).
[7] J. B. Goodenough, Annu. Rev. Mater. Res. **33**, 91 (2003).
[8] L. Chen, C. L. Chen, X. Chen, W. Donner, S. W. Liu, Y. Lin, D. X. Huang, and A. J. Jacobson, Appl. Phys. Lett. **83**, 4737 (2003).
[9] D. X. Huang, C. L. Chen, and A. J. Jacobson, Appl. Phys. Lett. **97**, 043506 (2005).
[10] S. Sanna, V. Esposito, D. Pergolesi, A. Orsini, A. Tebano, S. Licoccia, G. Balestrino, and E. Traversa, Adv. Funct. Mater. **19**, 1713 (2009).
[11] J. L. M. Rupp, A. Infortuna, and L. J. Gauckler, J. Am. Ceram. Soc. **90**, 1792 (2007).
[12] T. Suzuki, I. Kosacki, and H. U. Anderson, Solid State Ionics **151**, 111 (2002).
[13] I. Kosacki, T. Suzuki, V. Petrovsky, and H. U. Anderson, Solid State Ionics **136–137**, 1225 (2000).
[14] I. Kosacki, C. M. Rouleau, P. F. Becher, J. Bentley, and D. H. Lowndes, Solid State Ionics **176**, 1319 (2005).
[15] S. J. Litzelman and H. L. Tuller, Solid State Ionics **180**, 1190 (2009).
[16] E. Ruiz-Trejo, J. D. Sirman, Y. M. Baikov, and J. A. Kilner, Solid State Ionics **113–115**, 565 (1998).
[17] V. Boffa, V. Petrisor, L. Cointea, U. Gambardella, and S. Barbanera, Physica C **260**, 111 (1996).
[18] H. Wang, S. R. Foltyn, P. N. Arendt, Q. X. Jia, Y. Li, and Y. Zhang, Physica C: Superconducitivity **433**, 43 (2005).
[19] L. Chen, C. L. Chen, D. X. Huang, Y. Lin, X. Chen, and A. J. Anderson, Solid State Ionics **175**, 103 (2004).
[20] A. Infortuna, A. Harvey, and L. Gauckler, Adv. Funct. Mater. **18**, 127 (2008).
[21] V. Esposito and E. Traversa, J. Am. Ceram. Soc. **91**, 1037 (2008).
[22] M. Sillassen, P. Eklund, N. Pryds, E. Johonson, U. Helmersson, and J. Bøttiger, Adv. Funct. Mater. **20**, 2071 (2010).
[23] K. Otsuka, A. Kuwabara, A. Nakamura, T. Yamamoto, K. Matsunaga, and Y. Ikuhara, Appl. Phys. Lett. **82**, 877 (2003).